

A CRYSTAL-CHEMICAL STUDY OF CORDIERITE, SYNTHESIS AND STABILITY AT VARIABLE H₂O AND CO₂ CONCENTRATION: GEOLOGICAL AND TECHNOLOGICAL APPLICATIONS

FRANCESCO RADICA

Dipartimento di Scienze, Università Roma Tre, Largo San Leonardo Murialdo 1, 00154 Roma

INTRODUCTION

Cordierite is a relatively widespread mineral, having a peculiar ability to trap H₂O and CO₂ up to very high pressure and temperature. This is a unique property for a rock forming silicate, and has a significant role in the mineralogical equilibria in *HT* and *UHT* metamorphism (Harley & Thompson, 2004). In this PhD work, great attention was paid to the study of the diffusion mechanisms of carbon dioxide inside these channel-like structures. Considering that carbon dioxide is probably one of the major responsible for long-term climate change on Earth, the ability of these minerals to entrap CO₂ could provide insights for future research for the permanent CO₂ storage in minerals.

The aim was to investigate the diffusion of CO₂ across cordierite, and address possible implications from both a geological and a technological point of view. The work was completed by the parallel study of beryl, which is structurally related to cordierite.

EXPERIMENTAL AND DISCUSSIONS

Structural and spectroscopic characterization of cordierite

Eight different cordierite samples from different localities and geological occurrences were chosen to cover a wide range in H₂O/CO₂ ratio.

Single-crystal X-ray diffraction data were collected on optically clean grains, free from inclusions and alteration products, revealing all samples to be orthorhombic *Cccm*. Major oxides were analyzed by EMPA whereas H and C were quantified by SIMS (secondary ion mass spectrometry).

Optically transparent single-crystals were oriented using the spindle-stage and examined by FTIR micro-spectroscopy under polarized light. The observed bands were assigned to water molecules in two different orientations H₂O^[I] and H₂O^[II], and to CO₂ molecules in the structural channels. Prior to the quantitative analyses, the samples were examined for their water and carbon dioxide distribution using a focal-plane-array (FPA) of detectors. The evidence was that at the μm-scale the distribution of H and C in cordierite was significantly inhomogeneous, particularly for H₂O, whose zoning within the crystal can be strongly affected by the geological history of the mineral after its formation.

For H₂O the integrated molar coefficients for type I and type II water molecules were derived separately and turned out to be $^{[I]}\epsilon = 5000 \pm 1000 \text{ l}\cdot\text{mol}^{-1}\cdot\text{cm}^{-2}$ and $^{[II]}\epsilon = 13200 \pm 500 \text{ l}\cdot\text{mol}^{-1}\cdot\text{cm}^{-2}$, respectively. For CO₂ the integrated coefficient is $\epsilon_{\text{CO}_2} = 19000 \pm 1000 \text{ l}\cdot\text{mol}^{-1}\cdot\text{cm}^{-2}$ (see also Della Ventura *et al.*, 2012).

The same procedure was applied to the Fe end-member of the cordierite group, sekaninaite. Additional to FTIR single crystal X-ray refinement, laser ablation mass-spectroscopy for Li⁺ and Raman spectroscopy characterization were performed on this sample. X-ray site occupancy refinement suggested that the lack of monovalent charge at the octahedral site, due to the presence of Li⁺, is counter-balanced by the presence of Na⁺ in the channel.

Using the Beer-Lambert relation, integrated molar coefficients ϵ_i were calculated for both types of H₂O ($\epsilon_i \text{ H}_2\text{O}^{[I]} = 6000 \pm 2000$; $\epsilon_i \text{ H}_2\text{O}^{[II]} = 13000 \pm 1000$) and for CO₂ ($\epsilon_i \text{ CO}_2 = 2000 \pm 1000$) (see Radica *et al.*, 2013).

In-situ HT-IR spectroscopy and kinetic study of CO₂ expulsion from cordierite

Using a Linkam TS 1400 XY heating stage fitted on the FTIR microscope, I studied the *in situ* HT-FTIR micro-spectroscopy of cordierite and evaluated the kinetic and diffusion parameters of CO₂ expulsion as a function of increasing T.

Step-heating experiments on (001) oriented sections revealed that up to T > 800 °C there is a significant intensity increase of the CO₂ stretching mode at 2348 cm⁻¹, followed by a sudden decrease for T > 900 °C; the absorbance is virtually zero at 1000 °C (Fig. 1a). On the opposite, the integrated absorbance (A_i) of the CO₂ (ν₃ + ν₁) combination mode at 3708 cm⁻¹ (Fig. 1a) is almost constant up to about 450 °C, then decrease up to 850 °C. For higher T the intensity decreases with a much faster rate; the band disappears at 950 °C. Similar trends for the (010) section cut out from the same cordierite crystal (Fig. 1c).

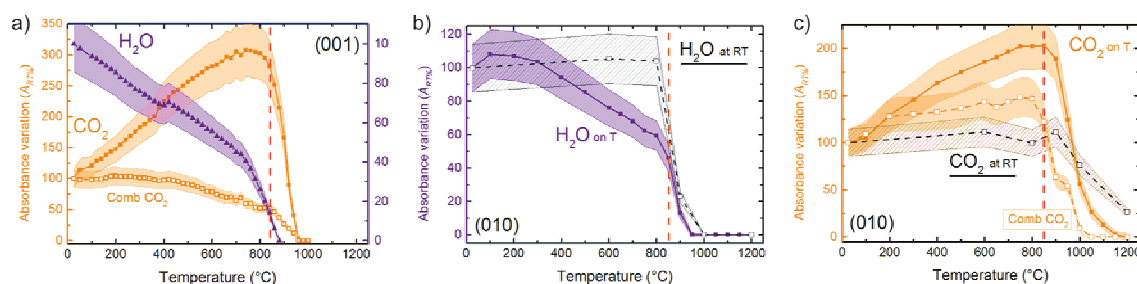


Fig. 1 - a) Cordierite (001) oriented section: integrated absorbance variation ($A_{RT}\%$ in %) of H₂O (purple triangles), CO₂ stretching mode (filled orange squares) and CO₂ combination mode (open orange squares); b and c) cordierite (010) oriented section: integrated absorbance variation ($A_{RT}\%$ in %) of H₂O (b) and CO₂ (c) absorptions. In Fig. 1b and Fig. 1c the intensities measured after quenching the sample are given for comparison (dashed black lines). The shaded areas represent the estimated error on $A_{RT}\%$.

The evolution of the H₂O absorbance as a function of increasing T is extremely different to that of CO₂ (Fig. 1a and b, in purple), and shows a linear and constant decrease of ~50% of the intensity up to 800 °C; in the 750-900 °C range there is a sudden drop. At 950 °C both samples are completely anhydrous. Similarly to what observed for CO₂, the data collected on quenched samples show a different scenario: the integrated H₂O absorbance is constant up to 800 °C and suddenly drops in the 800-900 °C range. At 1000° the sample is completely anhydrous.

Several authors (*e.g.*, Zhang *et al.*, 2007; Tokiwai & Nakashima, 2010) revised recently the absorbance in minerals and glasses in HT-FTIR spectroscopy and showed that the intensity measured during *in situ* experiments is not related to the concentration of the target absorber via the same Beer-Lambert relationship calibrated at room-T. This feature is shown in Fig. 1, where it is evident that *in situ* FTIR data collection does not provide a real estimate of the CO₂ and H₂O behavior in cordierite as a function of increasing T. In particular, based on the Beer-Lambert relationship, assuming no or negligible change in the sample thickness across the studied T range, the trends of Fig. 1 suggest a significant change in the molar absorption coefficients ϵ for both volatile species at varying T.

Continuous heating experiments were performed on (001) oriented cordierite slabs. Two fragments were double-polished at 60 μm and 19 μm , respectively and broke up into four pieces each. The four fragments of the same 60 μm thick section were heated to 850, 900, 950 and 1000 °C and kept at the target T for two hours. Additional four fragments of the 19 μm thick slab were heated to 825, 850, 900 and 1000 °C at different annealing times. Polarized spectra were collected every 5/10 minutes. The curves of residual CO₂ were fitted using three different approaches: the Avrami JMAK rate equation (Hancock & Sharp, 1972), the Avrami Putnis rate equation (Putnis, 1992) and the mono-dimensional plane sheet diffusion (Ingrin *et al.*, 1995).

Activation energies, calculated using the Avrami approaches, yield four different results on the basis of the used formula and the sample thickness. However, based on different assumptions, it is possible to conclude that the most reliable activation energy for CO₂ expulsion from cordierite provided by the Avrami formalism is $E_a = 138 \pm 12$ kJ/mol, *i.e.*, the value obtained using the Avrami Putnis equation on the thinner sample data set. This value is very close to those obtained by previous authors for the dehydration of cordierite (Giampaolo & Putnis, 1989). Using the mono-dimensional plane sheet diffusion approach it was possible to evaluate both the diffusion coefficient D and the activation energy E_a for CO₂ in cordierite. Results confirmed that this approach is not influenced by sample thickness variation and fitted data for both sample set yield a value of $-\log D_0 = 4.4 \pm 0.7$ m²/sec and $E_a = 204 \pm 15$ kJ/mol.

Experimental diffusion of CO₂ in cordierite and beryl at different PTt conditions

In this section I examined the interaction of cordierite with a CO₂-rich fluid under different experimental P, T, t conditions and evaluated the diffusion coefficients within the crystals. Experiments were performed using a non-end loaded piston cylinder apparatus (QUICKpress™ design by Depths of the Earth Co.).

Several cordierite fragments (Mg-cordierite from Karur, Tamil Nadu) were separated from a large single crystal and pre-treated at 1250 °C for 24 hours in order to remove all H₂O and CO₂ from the sample. The grains were optically clean, however cracking of larger grains occurred during the heat-treatment. The beryl samples were from the very first flux-grown synthetic emeralds made by P.G. Hautefueille and A. Perrey in 1888 in Paris (Bellatreccia *et al.*, 2008) and show a perfect prismatic hexagonal habitus.

The experiments were carried in 3×9 mm Pt capsules; silver carbonate was used as a CO₂ source. Experiments were performed in the pressure range 200 - 700 MPa, temperature range 700-900 °C; run duration varied from 1 to 72 hours.

Preliminary FTIR single spot measurements confirmed that H₂O and CO₂ diffusion in the samples (Fig. 2), however an evident heterogeneity in carbon dioxide absorbance was observed. Therefore, all samples were carefully examined by FPA to locate the area suitable for analytical spots. In particular FPA imaging revealed that the CO₂ diffusion in both cordierite and beryl proceeds exclusively along the structural channels parallel to the *c* axis (Fig. 3). FPA images also showed a strong enhancement of the CO₂ diffusion along cracks.

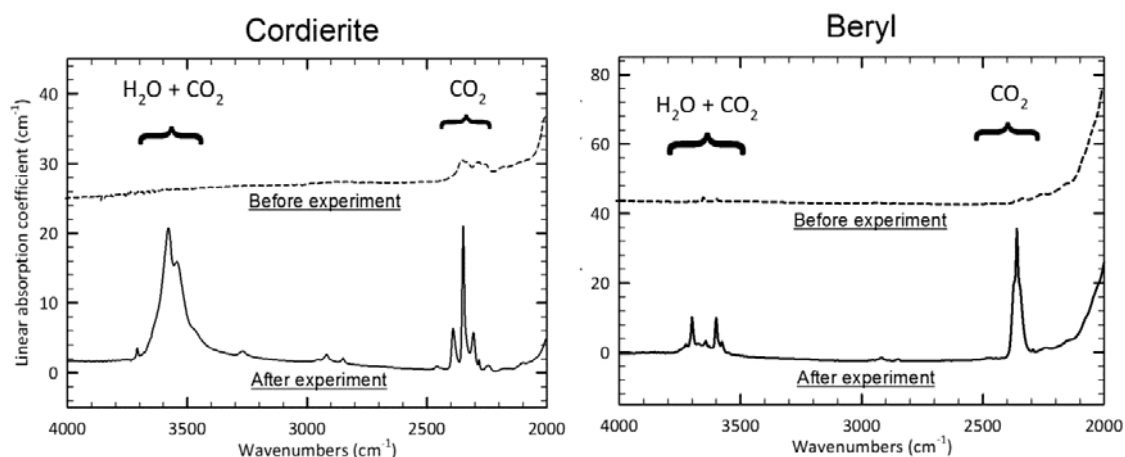


Fig. 2 - Unpolarized single-crystal spectra of a cordierite before and after treated at 900 °C and 500 MPa for 1 hour (left); unpolarized single-crystal spectra of a beryl before and after treated at 800 °C and 500 MPa for 10 hours (right).

On the basis of these results we located the most suitable area for the analytical spots avoiding measurements close to fractures; the beam size was kept as small as possible, usually at 20×20 μm² and the highest absorbance values were selected as representative of the CO₂ content of the sample. The CO₂ contents

were calculated from polarized FTIR spectra using the Beer-Lambert relationship and the procedure described in Della Ventura *et al.* (2012).

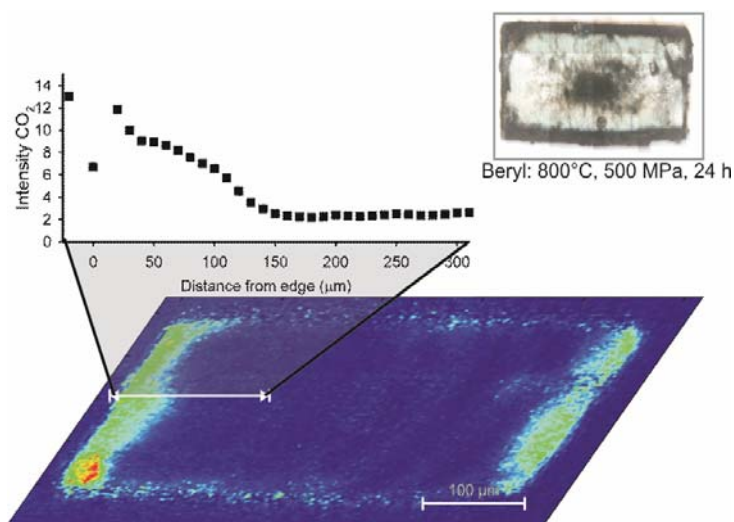


Fig. 3 - FPA image and FTIR diffusion profile of beryl treated at 800°C and 500 MPa for 24 hours.

Final data shows that *T* plays only a minor role on the CO₂ solubility for both cordierite and beryl, whereas pressure has a significant effect. In particular, beryl shows a steep increase in CO₂ content from 200 MPa to 500 MPa and from 500 MPa to 700 MPa. The CO₂ contents in cordierite, on the other side, show only a minor increase from 200 MPa to 500 MPa, with a significant jump from 500 MPa to 700 MPa.

The diffusion coefficient (*D*) for beryl was obtained by fitting the concentration profiles (Fig. 3) using a simple mono dimensional equation (Zhang & Cherniak, 2010):

$$C = C_0 \cdot \operatorname{erfc}\left(\frac{x}{2\sqrt{Dt}}\right)$$

where *C* is the concentration at depth *x* (m) from the sample rim, *C*₀ is the maximum concentration, *D* is the diffusion coefficient (m²/s), *t* is the time duration (s), and *erfc* is the complementary error function. Obtained *D* values for beryl range from 1.1E⁻¹⁴ to 9.5E⁻¹⁴.

Activation energy (*E*_a = 122 ± 15 kJ/mol) and pre-exponential factor (-log*D*₀ = 7.2 ± 0.7) for beryl were determined fitting the data on the basis of the Arrhenius equation.

Volatiles diffusion in hourglass zoned beryl and the coordination environment of H₂O in low-water samples

Some synthetic samples used for the diffusion experiments had a typical hourglass structure due to the distribution of Cr during the crystal growth (*e.g.*, Bellatreccia *et al.*, 2008). After the experimental run, the FTIR-FPA imaging of these sample showed an unexpected distribution of the diffused molecules within the channels (Fig. 4): CO₂ apparently diffuses following the hourglass boundaries, while H₂O^[II] is homogeneously distributed except along the hourglass traces.

Considering that the carbon dioxide diffusion in beryl and cordierite is significantly enhanced by the presence of fractures we performed high-resolution FESEM imaging to check for the possible presence of physical discontinuities across the hourglass boundary. The results showed that indeed the hourglass structure was exclusively due to a chemical zoning, thus suggesting that the diffusion pattern of CO₂ observed in Fig. 4 must be related to a kind of defect fast-path diffusion mechanism (Zhang *et al.*, 2006).

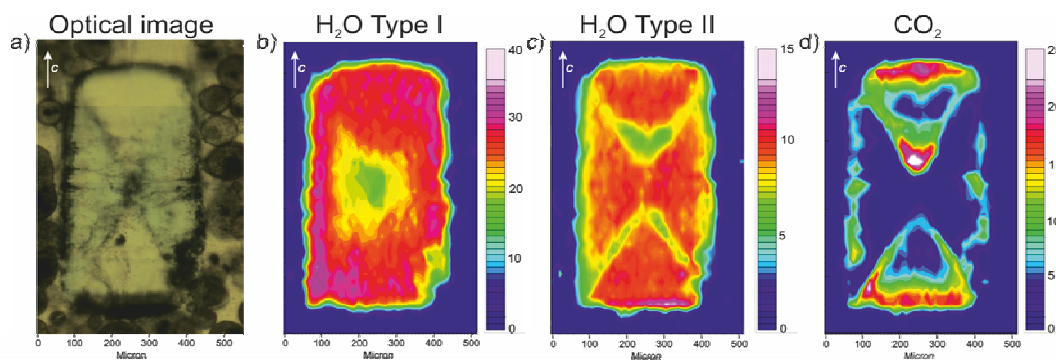


Fig. 4 - Polarized light FPA images of the beryl sample treated for four days at 800 °C, 500 MPa; a) optical image of the grain; b) E//c FTIR-FPA map of H₂O^[I]; c) E//c FTIR-FPA map of H₂O^[II]; (d) E⊥c FPA map of CO₂. Chromatic scale is proportional to CO₂ content.

The HT/HP experiments aimed at the CO₂ diffusion across cordierite and beryl were done using a piston-cylinder apparatus, where the pressure was mechanically and not hydrothermally increased. The infrared spectra of the run products, as expected, showed the presence of significant CO₂ but also of minor H₂O; due to the experimental conditions, this water content must be related to moisture present in the starting products used for the synthesis, thus its bulk amount is very low. Single-spot spectra collected along profiles parallel to the *c* crystallographic axis show subtle changes as a function of the distance from the crystal edge; these changes can be correlated to a progressive change in the H₂O coordination environment in the channel (Fig. 5), as a response to the varying H₂O/alkali content. In particular, the data show that when 2•H₂O > Na⁺ a.p.f.u., H₂O can assume both type I and type II orientation; in the latter case, each Na cation coordinates two H₂O^[II] molecules (doubly coordinated H₂O). If 2•H₂O < Na⁺ a.p.f.u., than H₂O^[II] molecules are singly coordinated to each Na cation. The same type of feature is observed and commented for the structurally related cordierite.

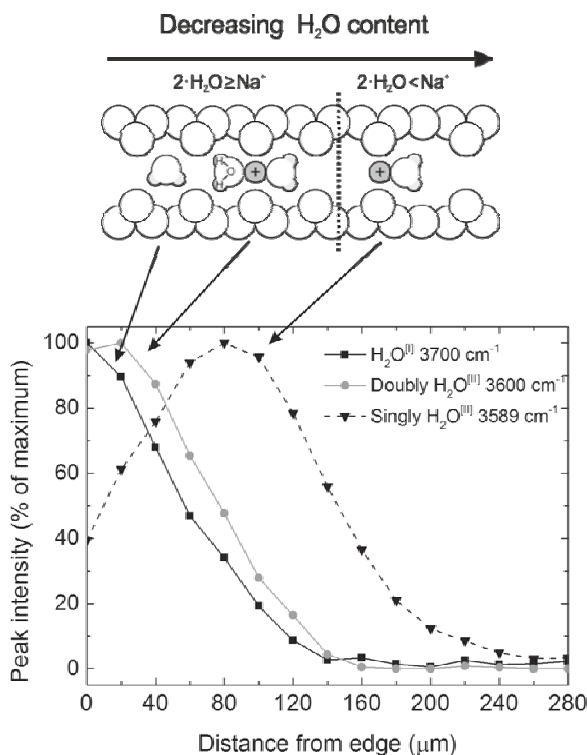


Fig. 5 - Top: schematic representation of the configuration of water molecules inside the structural channels of beryl, as the overall water content decreases. Bottom: concentration trend of selected peak for the beryl sample treated at 800 °C. Peak intensity were scaled to the maximum intensity.

The implication of this finding is that H₂O in beryl and in cordierite is trapped in the structural channel following very different bonding environments, and this has a significant consequence on the diffusion rates (both inward and outward) obtained in experiments and hence on the calculation of thermodynamic properties from the observed data. For cordierite in particular, considering it is widely used in metamorphic petrology as an indicator of the fluid system in equilibrium with the rock, the different diffusion mechanisms of water and CO₂ could affect the closing temperatures modeled on the basis of field studies (Della Ventura *et al.*, 2015).

CONCLUSIONS

This PhD Thesis was aimed at investigating the ability of cordierite and beryl, considered as a model for microporous materials, to diffuse and trap H₂O and CO₂ within their structural channels.

The work focused in particular on the CO₂ diffusion because of very few and controversial results so far available in the literature. In addition, CO₂ is considered one of the major cause of long-term climate change, thus knowledge of the conditions under which it diffuses into minerals may have interesting bearings for the design of new materials for the permanent storage of this gas. The study was done by combining different analytical techniques, however most data were based on micro-FTIR and FTIR-FPA imaging. Indeed, during this work novel applications of the FPA imaging were developed and tested for the first time in the study of Earth Science materials, in particular under polarized and synchrotron radiation.

The volatile-free crystals were treated at different pressure and temperatures in a CO₂ rich atmosphere using a non end-load piston-cylinder press, especially designed for short term experiments. The results showed that CO₂ diffusion inside beryl and cordierite proceeds exclusively along the structural channels running parallel to the *c* crystallographic axis, the same mechanism occurs also during CO₂ expulsion from the matrix. Thus the CO₂ loss from cordierite and beryl is strongly affected by both the particle size and shape of the crystal, *i.e.*, the length of the escape path. Fractures inside the grains also acted as additional pathways of inward and/or outward CO₂ diffusion, in accelerating the CO₂ diffusion across the grain. A third additional way of diffusion was observed in synthetic beryl. The planar defect generated by the structural mismatch in correspondence of the hourglass zoning also acted as a fast-path for CO₂ diffusion. A direct conclusion is that the simultaneous occurrence of different mechanisms may complicate the evaluation of diffusion coefficients of a molecular species, thus inspection of the distribution of a molecule inside the mineral via 2D imaging is mandatory in experimental work.

A major result of the solubility experiments described is that pressure plays a major role in controlling the amount of CO₂ diffused in both cordierite and beryl, whereas temperature and time have a minor effect, in line with data from natural occurrences (Thompson, *et al.*, 2001; Harley *et al.*, 2002). Surprisingly, however, the CO₂ contents introduced during the present study into cordierite were at least one order of magnitude lower than expected (Johannes & Schreyer, 1981; Armbruster & Bloss, 1982).

Cracks and fractures, produced during the thermal treatment, were found to enhance significantly the CO₂ diffusion with contents up to 4 times higher than at the edge of the grain. This feature has a great relevance from a technological point of view, because it demonstrates that to trap faster and larger CO₂ amounts inside the material, the use of highly fractured or clusters of micron-sized grains is preferred over larger grains.

Because of the well-developed hexagonal prismatic habitus, the beryl samples were excellent candidates to evaluate the inward diffusivity of CO₂ in microporous structures; diffusion coefficients for cordierite, on the opposite, could be evaluated only for the outward diffusion. As we may observe from Fig. 5 the diffusing rates calculated for CO₂ and H₂O (Fukuda *et al.*, 2009) in beryl are very close, even though CO₂ molecule are larger than the H₂O molecule. On the other hand, the inward CO₂ diffusion coefficients for beryl are larger than those calculated for the outward CO₂ diffusion in cordierite, even though the structures are very similar. Vry *et al.* (1990) observed that in cordierite inward diffusion is quicker than outward diffusion. These authors stated that the difference between inward and outward diffusion rates may be caused by alkali cations and CO₂ itself, that, acting as plugs in the channel, preferentially slows down outward volatile diffusions.

In Fig. 6 we may observe that the diffusion coefficients measured for CO₂ in beryl are close to the OH⁻ diffusion coefficients obtained in other ring silicates like tourmaline (Desbois & Ingrin, 2007), layer silicates like muscovite (Graham, 1981), amphiboles like kaersutite (Ingrin & Blanchard, 2000), or in disilicates like epidote (Graham, 1981). However, it is important to note that OH⁻ groups probably diffuses inside these structures in the form of H⁺ (Zhang & Cherniak, 2010) thus the diffusing species is much smaller compared to molecular CO₂ and H₂O.

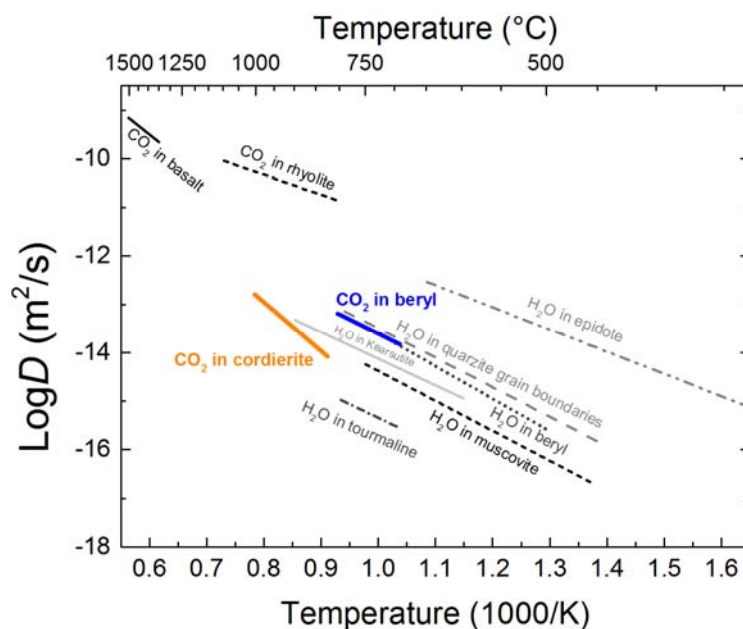


Fig. 6 - Arrhenius diagram of various diffusion coefficients D for different silicates or silicate melts for H₂O and CO₂ (D for beryl after diffusion profiles and D for cordierite after isothermal heating experiments).

Our data suggest that the structural channels of cordierite and beryl act more likely as fast paths for the mobility of large molecular groups compared to similar silicate structures, and for this reason the diffusing behavior is more similar (in terms of diffusion coefficients, not in the mechanism) to the one typically observed for grain boundary diffusion, such as, for example, H₂O in quartzite (Farver & Yund, 1991) or to the behavior of CO₂ in non-crystalline materials, like silicate melts (Watson *et al.*, 1982).

REFERENCES

- Armbruster, T. & Bloss, F.D. (1982): Orientation and effects of channel H₂O and CO₂ in cordierite: *Am. Mineral.*, **67**, 284-291.
- Bellatreccia, F., Della Ventura, G., Piccinini, M., Grubessi, O. (2008): Single-crystal polarized light IR study of an historical synthetic water poor emerald. *N. Jb. Miner. Abh.*, **185**, 11-16.
- Della Ventura, G., Radica, F., Bellatreccia, F., Cavallo, A., Capitelli, F., Harley, S. (2012): Quantitative analysis of H₂O and CO₂ in cordierite using polarized FTIR spectroscopy. *Contrib. Mineral. Petrol.*, **164**, 881-894.
- Della Ventura, G., Radica, F., Bellatreccia, F., Freda, C., Cestelli Guidi, M. (2015) Speciation and diffusion profiles of H₂O in water-poor beryl: comparison with cordierite. *Phys. Chem. Miner.*, Accepted.
- Desbois, G. & Ingrin, J. (2007): Anisotropy of hydrogen diffusion in tourmaline. *Geochim. Cosmochim. Acta*, **71**, 5233-5243.
- Farver, J.R. & Yund, R.A. (1991): Measurement of oxygen grain boundary diffusion in natural, fine grained, quartz aggregates. *Geochim. Cosmochim. Acta*, **55**, 1597-1607.
- Fukuda, J., Shinoda, K., Nakashima, S., Miyoshi, N., Aikawa, N. (2009): Polarized infrared spectroscopic study of diffusion of water molecules along structure channels in beryl. *Am. Mineral.*, **94**, 981-985.
- Giampaolo, C. & Putnis, A. (1989): The kinetics of dehydration and order-disorder of molecular H₂O in Mg-cordierite. *Eur. J. Mineral.*, **1**, 193-202.

- Graham, C.M. (1981): Experimental hydrogen isotope studies III: Diffusion of hydrogen in hydrous minerals, and stable isotope exchange in metamorphic rocks. *Contrib. Mineral. Petr.*, **76**, 216-228.
- Hancock, J.D. & Sharp, J.H. (1972) Method of Comparing Solid-State Kinetic Data and Its Application to the Decomposition of Kaolinite, Brucite, and BaCO₃. *J. Am. Ceram. Soc.*, **55**, 74-77.
- Harley, S.L. & Thompson, P. (2004): The influence of cordierite on melting and mineral-melt equilibria in ultra-high-temperature metamorphism. *T. Roy. Soc. Edin-Earth*, **95**, 87-98.
- Harley, S.L., Thompson, P., Hensen, B.J., Buick, I.S. (2002): Cordierite as a sensor of fluid conditions in high-grade metamorphism and crustal anatexis. *J. Metamorph. Geol.*, **20**, 71-86.
- Ingrin, J. & Blanchard, M. (2000): Hydrogen mobility in single crystal kaersutite. EMPG VIII, *J. Conference Abs.*, **5**, 52.
- Ingrin, J., Hercule, S., Charton, T. (1995): Diffusion of hydrogen in diopside: results of dehydration experiments. *J. Geophys. Res.*, **100**, 15489-15499.
- Johannes, W. & Schreyer, W. (1981): Experimental introduction of CO₂ and H₂O into Mg-cordierite. *Am. J. Sci.*, **281**, 299-317.
- Putnis A. (1992): Introduction to mineral science. Cambridge University Press, 457 p.
- Radica, F., Capitelli, F., Bellatreccia, F., Della Ventura, G., Cavallo, A., Piccinini, M., Hawthorne, F.C. (2013): Spectroscopy and X-ray structure refinement of sekaninaite from Dolní Bory (Czech Republic). *Mineral. Mag.*, **77**, 485-498.
- Thompson, P., Harley, S.L., Carrington, D.P. (2001): The distribution of H₂O-CO₂ between cordierite and granitic melt under fluid-saturated conditions at 5 kbar and 900 °C. *Contrib. Mineral. Petr.*, **142**, 107-118.
- Tokiwai, K. & Nakashima, S. (2010): Integral molar absorptivities of OH in muscovite at 20 to 650 °C by *in-situ* high-temperature IR microspectroscopy. *Am. Mineral.*, **95**, 1052-1059.
- Vry, J.K., Brown, P.E., Valley, J.V. (1990): Cordierite volatile content and the role of CO₂ in high-grade metamorphism. *Am. Mineral.*, **75**, 71-88.
- Watson, E.B., Sneeringer, M.A., Ross, A. (1982): Diffusion of dissolved carbonate in magmas: experimental results and applications. *Earth Planet. Sci. Lett.*, **61**, 346-358.
- Zhang, X.Y., Cherniak, D.J., Watson, E.B. (2006): Oxygen diffusion in titanite: lattice diffusion and fast-path diffusion in single crystals. *Chem. Geol.*, **235**, 105-123.
- Zhang, M., Salje, E.K.H., Carpenter, M.A., Wang, J.Y., Groat, L.A., Lager, G.A., Wang, L., Beran, A., Bismayer, U. (2007): Temperature dependence of IR absorption of hydrous/hydroxyl species in minerals and synthetic materials. *Am. Mineral.*, **92**, 1502-1517.
- Zhang, X.Y. & Cherniak, D.J. (eds.) (2010): Diffusion in Minerals and Melts. *Rev. Mineral. Geochem.*, **72**, 1036 p.